Annals of Glaciology

Article

Cite this article: Fegyveresi JM, Alley RB, Buizert C, Fitzpatrick JJ, Courville ZR, Voigt DE (2025) Temperature reconstruction from measured bubble number-density evolution in the South Pole Ice Core since the late-glacial (~19.5 ka). *Annals of Glaciology* **66**, e25, 1–11. https://doi.org/10.1017/aog.2025.10011

Received: 19 January 2025
Revised: 24 April 2025
Accepted: 16 May 2025

Keywords:
glacier modeling; ice and climate; ice core; ice physics; paleoclimate

Corresponding author: John M. Fegyveresi; Email: john.fegyveresi@nau.edu

© The Author(s), 2025. Published by Cambridge University Press on behalf of International Glaciological Society. This is an Open Access article, distributed under the terms of the Creative Commons Attribution licence (http://creativecommons.org/licenses/by/4.0), which permits unrestricted re-use, distribution and reproduction, provided the original article is properly cited.

cambridge.org/aog

Temperature reconstruction from measured bubble number-density evolution in the South Pole Ice Core since the late-glacial (~19.5 ka)

John M. Fegyveresi[1], Richard B. Alley[2], Christo Buizert[3], Joan J. Fitzpatrick[4], Zoe R. Courville[5] and Donald E. Voigt[2]

[1]School of Earth and Sustainability, Northern Arizona University, Flagstaff, AZ, USA; [2]Department of Geosciences, and Earth and Environmental Systems Institute, The Pennsylvania State University, University Park, PA, USA; [3]College of Earth, Ocean, and Atmospheric Sciences, Oregon State University, Corvallis, OR USA; [4]Geosciences and Environmental Change Science Center, U.S. Geological Survey, Denver, CO, USA and [5]US Army Corps of Engineers Engineer Research and Development Center, Cold Regions Research and Engineering Laboratory, Hanover, NH, USA

Abstract

We present analyses of bubble number-density (BND) data from the South Pole Ice Core (SPC14) showing warming of ~7.5°C from the Late Glacial (~19.5 ka), then relatively stable temperatures during the Holocene (<0.5°C warming), in close agreement with results of independent paleothermometers. The BND data span from ~160 m just below pore close-off, to ~1200 m, where bubble loss by clathrate formation is significant. Measurements were made with standard bubble 'thick'-section techniques and a new application of three-dimensional micro-computed tomography (CT) imagery; the nearly identical results recommend the faster, nondestructive micro-CT. The very high BND at South Pole, typically 800 and 900 bubbles cm^{-3}, reflects the joint effects of the relatively low mean-annual temperature (−49°C) and high accumulation rate (~7.5 cm w.e. a^{-1}). High BND is physically linked to small grain sizes at pore close-off, which in turn helps explain the near-absence of brittle-ice behavior at the site, contributing to the high quality of the recovered core with implications for siting of future ice cores. The accumulation history, derived from $\delta^{15}N\text{-}N_2$ firn-column thickness estimates, correlates with the temperature history but varies somewhat more than saturation vapor pressure, suggesting dynamic controls including upstream slope variability.

1. Introduction

Ice cores are incredible archives of paleoenvironmental data, containing crucial insights into past climate and supplementing and extending instrumental data (e.g. Schneider and Steig, 2008; Steig and others, 2009, Fegyveresi and others, 2011). Data from ice cores are especially valuable because they provide multiple, independent constraints on the history of key climatic variables such as temperature or snow accumulation rates (e.g. Alley, 2010; Cuffey and Paterson, 2010). Multiple ice-core proxies (e.g. stable isotopes, ice chemistry, etc.) have been used to develop indicators of past climates across multiple sites, and while these proxies are fairly well-established qualitatively, corroboration through independent data sets, as well as calibration of the geochemical paleo-thermometer, is invaluable for establishing robust and accurate paleoclimate reconstructions.

Spencer and others (2006) showed that estimates of past temperatures in polar ice can be quantitatively reconstructed from ice-core bubble number-density (BND) and site accumulation rates. Recent applications of this model employed for the West Antarctic Ice Sheet Divide site (Fegyveresi and others, 2011, 2016) validated the effectiveness and capability of this technique for establishing independent records down to the depth at which bubble loss to clathrate formation becomes significant, which in previous applications of the technique has been in Holocene ice. The use of this technique requires slow, labor-intensive bubble-section preparation and analyses.

Here, we present an independent paleoclimate reconstruction for South Pole across the most recent glacial termination, and up through the Holocene, using this BND paleoclimate indicator. We also present and compare data derived from a new three-dimensional (3-D) imaging technique developed using micro-CT technology. We show that using this new imaging technique instead of the traditional bubble-section imagery produces comparable results, with similar precision and uncertainty. In addition, this imaging technique is effectively nondestructive to the ice samples, and sample preparation and measurement is considerably more efficient, enabling faster and more-accurate future analyses.

Loss of bubbles to form clathrate hydrates in the South Pole core was insignificant in ice samples younger than ~20 ka (ka bf 1950), allowing the results here to give the first independent temperature reconstruction from BND through the glacial transition. This new temperature reconstruction for South Pole agrees with other independently derived reconstructions of surface temperatures for the site based on isotope proxies, diffusion length estimates and firn densification modeling (Buizert and others, 2021a; Kahle and others, 2021).

2. Background

2.1. South Pole site specifics

The main coring of the South Pole Ice Coring Project (SPICEcore) took place over two Antarctic summer seasons between 2014 and 2016. The drilling site, located at 89.99° S, 98.16° W and ~2 km from the primary South Pole Station, is unique in that the mean annual temperature at the drilling location (−49°C) is more typical of East Antarctic sites, while the mean accumulation rate (~7.5 cm w.e. a^{-1}) is more typical of West Antarctic sites (Casey and others, 2014). The site has an estimated ice thickness of 2700 m, an ice velocity of 10 m a^{-1} along 40°W, is situated at ~2835 m above sea level, and has an estimated depth to pore close-off of ~120 m (Battle and others, 1996, Casey and others, 2014; Sneed and others, 2011). The primary recovered core, SPC14, was drilled to a depth of 1751 m, with the ice dated to ~54 300 years BP (Winski and others, 2019). Calculated gas-age/ice-age differences for the core were as high as 2500 years, with gas-ages at the bottom of the core of ~52 500 years BP (Epifanio and others, 2020).

Several studies have been published recently reconstructing glaciological, chemical and temperature histories for the South Pole site using the primary SPC14 core. These include analyses of accumulation (Fudge and others, 2016; Kahle and others, 2021), advection and ice-provenance trends (Lilien and others, 2018; Fudge and others, 2020), oxygen isotope trends (Markle and others, 2018; Steig and others, 2021; Markle and Steig, 2022) and trapped gas trends (Epifanio and others, 2020; Morgan and others, 2022; Epifanio and others, 2023). The temperature reconstructions published thus far for the South Pole site have used several proxies, including the well-known water stable isotope thermometer (Markle and Steig, 2022), isotope diffusion lengths (Kahle and others, 2021) and the history of firn densification at the site (Buizert and others, 2021a). These reconstructions for South Pole have all revealed a general temperature increase across the recent glacial transition of between ~7°C and ~10°C.

An investigation of the visual stratigraphy was also carried out for the site (Fegyveresi and others, 2019a). Seasonal coarse-grained and depth-hoar layers were used to identify the annual layers (also see Gow, 1965), and the results reveal accumulation trends that could indicate past climatological or glaciological changes at the site. Specifically, one 1600 year interval from 6700 to 5100 years BP (years bf 1950) experienced a higher-than-average accumulation rate (~8.1 cm w.e. a^{-1}), while one 700 year interval from 3100 to 2400 years BP (years bf 1950) experienced a lower-than-average accumulation rate (~6.4 cm w.e. a^{-1}); several analyses have suggested these temporal patterns in the core are related to upstream spatial patterns in accumulation and redistribution of snow (Winski and others, 2021, Morgan and others, 2022).

Over 1900 individual wind or iced crusts were also observed and documented, as well as one visible tephra layer at a depth of 306.6 m in the core (~3560 years BP and likely tied to an eruption of Candlemas Island in the South Sandwich Islands; Palais and others, 1987). These data contributed to the accumulation-rate reconstruction that is needed in the BND temperature-reconstruction technique, and demonstrated, not surprisingly, that the core is ordinary bubbly ice suitable for that reconstruction.

2.2. BND paleothermometry

Even with the demonstrated success of known ice-core paleoclimate proxies (such as $\delta^{18}O_{ice}$), it is essential that any such proxy or its associated reconstruction technique or model be continually tested, refined, and improved to ensure that they are spatially and temporally robust across sites with differing paleo-histories and conditions. It is also valuable to develop complementary paleoclimate reconstructions using methods reliant on entirely independent variables, so as to better corroborate those reconstructions and affirm that they represent the most accurate temperature histories. A recent study showed that borehole thermometry in interior East Antarctica yields Last Glacial Maximum (LGM) temperature estimates significantly warmer than those estimated from the traditional use of water stable isotope ratios (Buizert and others, 2021a), providing a need for independently calibrated temperature proxies to resolve this discrepancy.

Based on the modeling in Alley and Fitzpatrick (1999), Spencer and others (2006) developed a technique that allows for the reconstruction of either paleotemperatures or paleo-accumulation rates by fitting a semiempirical steady-state model to measured number-densities of bubbles in ice cores. Polar firn densification is primarily driven by temperature and accumulation rate (Gow, 1968); however, during burial following pore close-off, ice grain sizes quickly become unreliable indicators of firnification conditions due to various processes that depend on other factors such as ice deformation rate (Spencer and others, 2006). Given that the geometry of firn at pore-close off is essentially self-similar (Gow, 1968), the integrated effects of temperature and accumulation rate on density and grain growth are therefore recorded in the number-density of bubbles formed as the firn is transformed into ice at the pore close-off depth (Spencer and others, 2001, 2006). Furthermore, due to slow gas diffusion between ice-core bubbles, BNDs in ice can reliably preserve information about firnification conditions over longer periods (Alley and Fitzpatrick, 1999).

Conserved number-density then allows for the use of the firn-densification and grain-growth models to invert for either the firnification paleotemperature or paleo-accumulation rate, provided the other parameter is known. This method was updated and applied successfully using ice-core data from the West Antarctic Ice Sheet (WAIS) Divide site, revealing an overall ~1.7°C Holocene cooling—with notable smaller climatic trends contained therein—that also agreed with $\delta^{18}O$ reconstructions (Fegyveresi and others, 2011, 2016).

As noted, the South Pole site experiences a unique combination of environmental variables for an Antarctic site, most notably its relatively high mean-annual accumulation rates for its relatively low mean-annual temperature (Casey and others, 2014). Both of these site conditions favor slower grain growth with depth, and therefore smaller mean grain and bubble sizes, as well as higher BND values (Gow, 1968). Combined with a higher-resolution annual stratigraphy as compared to other East Antarctic sites, it places South Pole into a 'sweet spot' with respect to BND, allowing for both a greater depth of resolvable annual layers, as well as the potential reconstruction of temperature histories back through the most-recent glacial termination into the Pleistocene (the Spencer

https://doi.org/10.1017/aog.2025.10011 Published online by Cambridge University Press

model has not yet been successfully applied to any ice core containing bubbly ice older than Holocene-aged). It is worth noting that the South Pole site is located in a flank-flow setting, and therefore the climatic record from deeper in the core represents conditions from farther upglacier, introducing the need for ice-flow corrections to answer certain paleoclimatic questions, with the associated uncertainties in ice flow (Fudge and others, 2016; Lilien and others, 2018) .

During field recovery of the SPC14 core, it was also observed that the core exhibited very minimal brittle-ice behavior, even at brittle-ice zone (BIZ) depths traditionally associated with extreme instability, fracturing and spalling (Souney and others, 2021; Fegyveresi and others, 2019a). Later, inspection of thin sections prepared from the core also revealed a nearly complete lack of any chessboard subgrain structures, likely arising in large part from the small grain sizes which in turn are controlled by the high accumulation rate and low temperature of the site. Recent work by Fitzpatrick and others (2024) and Barnett and others (2023) suggests that brittle behavior involves fracturing along the chessboard subgrain boundaries. This diminished brittle-ice behavior has implications for site-selection for future ice cores. It also was extremely favorable for more continuous and accurate BND measurements, as bubble-section preparation was less affected by cracking during the ice cutting and microtoming processes, resulting in more-pristine (and defect-free) imagery.

Because of the higher BND counts, lack of overall brittleness and smaller grains, the South Pole core is excellent for both applying and refining the Spencer model, and for testing new measurement techniques and methods. As noted by Fegyveresi and others, (2011, 2016), measurement of BND on bubble-sections introduces small uncertainties due to the two-dimensional (2-D) stereological projection of 3-D bubbles, which might be avoided with 3-D measurement techniques that capture true volumetric data and imagery, such as X-ray microtomography.

Over the past two decades, micro-computed tomography, or simply micro-CT, has been shown to be an effective tool for measuring 3-D properties of glacier ice without significant degradation to the sample (e.g. Hagenmuller and others, 2013; Dadic and others, 2019; Bagherzadeh and others, 2023). Micro-CT technology generates 3-D images composed of an integrated collection of 2-D projections, or 'slices', of the target specimen. At high enough resolution, this technique can therefore generate not just true 3-D counts of trapped bubbles in a given volume, but also volumetric size estimates of those bubbles. Here, we prepared 11 unique micro-CT samples at 100 m intervals (and from equivalent depths to those of traditional bubble-section sampling) as a way to test the efficacy and accuracy of the technology for measuring BND and mean bubble sizes. Our primary objective was to determine if this technique could be used as a viable alternative for ascertaining bubble counts, and ultimately, BND. We show that this new technique is viable and indeed nondestructive of the prepared samples, and can greatly reduce sample preparation and imaging processing time for future ice-core measurements.

3. Methods and data

3.1. Bubble number-density

To obtain both the ice-core bubble-sections and micro-CT sections, samples were first cut from the appropriate core depth sections in the National Science Foundation Ice Core Facility's −26°C ice preparation room. Following Fegyveresi and others (2011, 2016), we used a band saw to first cut thick bubble sections ~10 cm long by ~6 cm wide by 5 mm thick, at 20 m depth intervals ranging from 160 to 1200 m depth in the core. One face of each sample was smoothed with a sledge-type microtome and then affixed to a glass slide using a combination of silicone oil and tinkered water-ice. These samples were then microtomed to ~1.5 mm overall thickness and recorded with several overlapping high-resolution images using the on-site digital camera stage. Final imagery was stitched using *Adobe Photoshop* software to produce the high-resolution bubble-sections (e.g. Fig. 1). Estimates of BND were calculated—with appropriate bubble-cut corrections—following Fegyveresi and others (2011, 2016), and using the *QIA-64* (formerly *Fovea Pro*) image analysis plug-in for *Adobe Photoshop*.

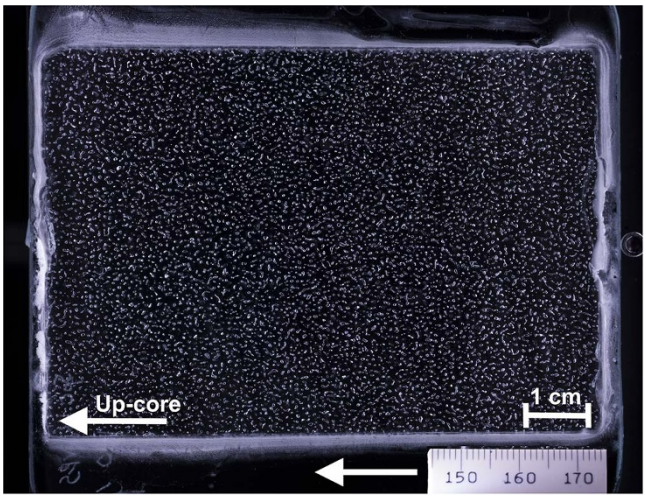


Figure 1. An unedited bubble-section image from the 160 m vertically oriented sample (just below pore close-off). Image shown with scale and stratigraphic core orientation.

Micro-CT samples were cut at 100 m intervals ranging from 200 to 1200 m depth. These samples measured 2.5 cm square, by 8 cm long and were split in half for replicate measurements. All micro-CT measurements were made on site in a − 10°C cold room at the Cold Regions Research and Engineering Lab in Hanover, NH. We used a Bruker SkyScan 1173 desktop micro-CT scanner with a Hamamatsu 130/300 tungsten X-ray source and flat-panel sensor camera detector, with samples mounted in standard plastic measurement containers (see, e.g. Fig. 2). The X-ray source of the SkyScan 1173 produces a fixed conical, polychromatic beam that operates a distortion-free X-ray detector with a source spot size of <5 μm, a spatial resolution detectability of <4 μm, and contrast resolution of <7 μm. For our measurements, we set the maximum accelerating voltage of the X-ray beam at 40 kV, with a current of 200 μA. Samples were rotated 180° in 0.35° steps, with five-frame averaged attenuation images captured at each step using a camera exposure of 400 ms. We used a 2 × 2 binning protocol to create final X-ray radiographs of 1120 × 1120 pixels. Reconstructions and analyses of these radiographs were carried out use the native Bruker software package NRECON, which uses a modified Feldkamp cone-beam algorithm to produce a vertical stack of gray-scale cross-section images. As part of the image post-processing, we performed ring artifact reduction, post-alignment and beam hardening corrections, and a two-pixel Gaussian kernel smoothing to reduce noise. The resulting images had a spatial resolution of 15 μm per voxel (e.g. Fig. 3). We selected a smaller

https://doi.org/10.1017/aog.2025.10011 Published online by Cambridge University Press



Figure 2. Bruker SkyScan 1173 X-ray micro-CT instrument located in a −10°C cold room at the Cold Regions Research and Engineering Laboratory. Scanner shown with a sample mounted in plastic specimen container on the measurement stage.

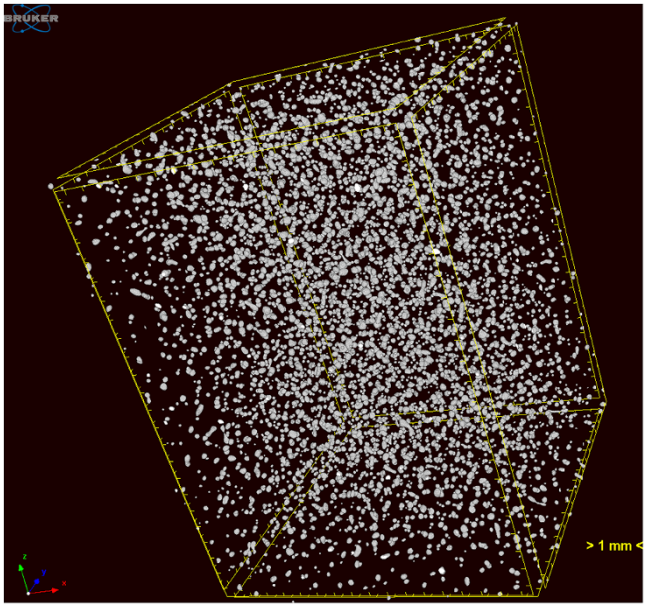


Figure 3. A volumetric 3-D rendering of micro-CT imagery for the sample taken from 300 m depth. Each small feature represents a bubble measured within the sample volume of interest.

internal volume of interest for analyses, measuring ~10 000 mm^3, in order to eliminate sample edge effects and gaps. We performed 3-D analyses on the resulting segmented images using Skycan CTAn software. Standard binary thresholding and 5-voxel despeckling algorithms were first applied to reduce image noise and eliminate non-bubble defects. Final returned data included all measured feature (bubble) counts and sizes. Overall measurement errors reflect a combination of analytical instrument uncertainty and the one sigma (1σ) standard of replicate samples.

BND is the number of bubble centers in a given volume of ice, but because of the finite size of bubbles, parts of some bubbles with centers outside of a sample will be observed in a sample. Standard correction methods have been developed for these 'cut bubbles', and were followed here (see Saltykov, 1976; Martinerie and others, 1990; Fegyveresi and others, 2011). We also followed Lipenkov (2000) and Ueltzhoffer and others (2010) in identifying and eliminating any 'microbubbles' from our bubble counts. In ice from especially cold sites such as South Pole, microbubbles can account for up to 20% of total observed bubbles (Lipenkov, 2000), although in our measured samples, they were never >5%. Consequently, the highest concentration of microbubbles we eliminated in any of our samples was 5% of the total bubble count, and errors in identification are a small fraction of that. Similar to WAIS Divide (Fegyveresi and others, 2016), for the purpose of using BND as a climate indicator, this small concentration was negligible.

We measured BND using the bubble-sections and micro-CT samples, with typical values ranging between 800 and 900 bubbles cm^{-3} over the clathrate-free portion of our sampling interval—with a maximum value of 938 bubbles cm^{-3} measured at depth of 500 m (Fig. 4). These number-densities are notably higher than published values from other ice-core sites (see, e.g. Spencer and others, 2006; Fegyveresi and others, 2011), reflecting the combined effects of the relative colder mean temperatures, and higher mean accumulation rates at South Pole. The onset of clathrates did begin to notably affect our data below ~1100 m, so for the purposes of our paleoclimate reconstruction, modeled temperatures from below this depth were considered unreliable. The glacial–interglacial transition, occurring between ~1100 and 800 m in depth, is not immediately obvious in the raw BND data. This is because the colder temperatures and lower accumulation rates during glacial periods have opposite effects on BND.

3.2. Accumulation-rate history

As noted above, reconstruction of paleotemperatures from BND data requires paleo-accumulation rates. Here, we describe our accumulation history after a short review of earlier work illustrating important characteristics of the site.

Beginning in 1965, several shallow firn and ice cores were drilled near South Pole Station (e.g. Gow, 1965; Giovinetto and Schwerdtfeger, 1965; Kuivinen, 1983; Mosley-Thompson and others, 1999), each resulting in slightly different modern mean accumulation-rate estimates, ranging between 5.0 and 8.5 cm w.e. a^{-1} (see also van der Veen and others, 1999; Casey and others, 2014). During the 2002–03 field season, the International Trans-Antarctic Scientific Expedition (ITASE) drilled a 207 m core ~8 km from the South Pole Station as part of their array of Antarctic cores. Visual stratigraphy was measured on this core in the field, yielding an accumulation rate of ~7.6 cm w.e. a^{-1} when averaged over the 207 m (A. Gow, pers. comm., 2015; Sneed and others, 2011). The most recent estimate of modern mean-accumulation rate derived from the SPC14 core is ~7.4 cm w.e. a^{-1}, ranging between ~7.0 and ~9.0 cm w.e. a^{-1} through the Holocene (Fegyveresi and others, 2019a; Winski and others, 2019).

Because the South Pole site is in a region of flank flow (not on an ice divide), with notable uncertainties in flow velocities over the history of accumulation of the ice in the core, the origin of measured accumulation can be somewhat complicated (Casey and others, 2014; Lilien and others, 2018). Estimated regional ice-flow velocities for South Pole range between 9.6 and ~10.1 m a^{-1} (Hamilton 2004; Bamber and others 2000), and therefore the provenance of any measured ice from deep within recovered cores at the site, is likely hundreds of kilometers upstream and sourced from a very large total catchment area.

https://doi.org/10.1017/aog.2025.10011 Published online by Cambridge University Press

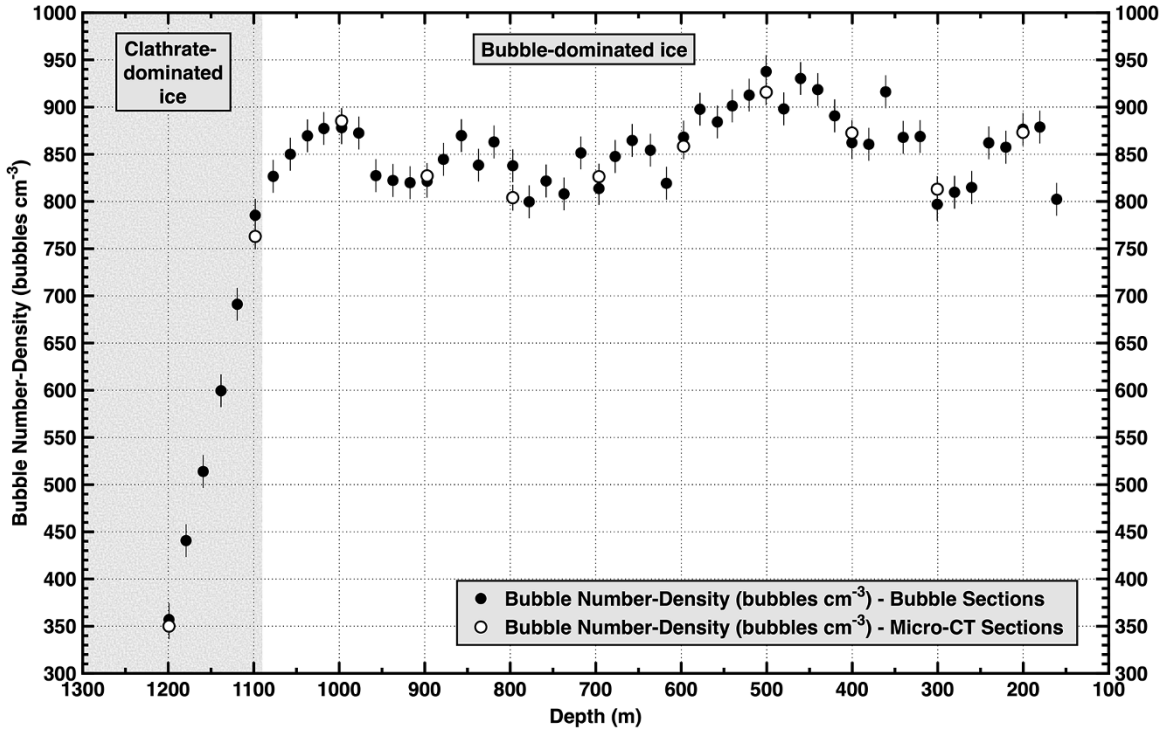


Figure 4. Measured bubble number-densities plotted against depth. Error bars represent estimated mean bubble count error across all samples. The clathrate-ice zone is shown in gray.

Deeper layers in the SPC14 ice core were deposited upstream of the current coring location; therefore, the effective accumulation rate (A) in the core reflects both past climatic changes and upstream patterns of snow accumulation (Lilien and others, 2018; Fudge and others, 2020). Variations in the latter appear well-correlated with the surface curvature, or second derivative of the surface elevation, along the flow path, suggesting a role of surface snow redistribution by katabatic winds (Morgan and others, 2022). The SPC14 (A) history has been reconstructed in various ways. Winski and others (2019) reconstructed Holocene accumulation rates based on annual layer thickness and a simple 1D Nye ice flow model (Nye, 1963). The advantage of this method is that it allows high temporal resolution; however, it relies on a simplified and somewhat poorly constrained ice-flow model. Kahle and others (2021) used a statistical inverse approach to simultaneously reconstruct a number of glacio-climatological parameters (A, T, thinning function) using empirical reconstructions of the water isotope diffusion length and the gas age-ice age difference (Δage). The advantage of this approach is that it covers the full length of the ice core; however, the method is not optimized for reconstructing past A, and it does not incorporate firn thickness information available from the isotopic composition of N_2 ($\delta^{15}N\text{-}N_2$). Here we use an empirical method to reconstruct A based on its fundamental relationship to firn thickness and firn age (Buizert, 2021b). Vertical gas diffusion within the firn pore network effectively stops at the lock-in depth L. At this depth, the gravitational isotopic enrichment of gases (such as $\delta^{15}N\text{-}N_2$) halts, and the Δage is fixed (Sowers and others, 1992). The ice-equivalent lock-in depth (L_{IE}) gives the amount of ice (in meters) above L, and is given by

$$L_{IE} = \int_0^L \rho(z)/\rho_{ice} dz \quad (1)$$

Over a wide range of climatic conditions, the ratio L_{IE}/L is constant and ~0.7 (Parrenin and others, 2012). Presently at South Pole, this ratio is 0.712 (Vandecrux and others, 2023). The SPC accumulation rate is therefore given by

$$A = \frac{L_{IE}}{\Delta age} = \frac{L}{0.712 \times \Delta age} \quad (2)$$

For SPC, the Δage has been empirically reconstructed by combining volcanic synchronization of the ice ages, and methane synchronization of the gas ages to the WAIS Divide ice core that has an accurate layer-counted chronology and a small Δage (Buizert and others, 2015; Epifanio and others, 2020; Sigl and others, 2016). In our reconstruction, we add 25 years to the published empirical Δage values to account for the diffusive age of the gases and thereby estimate the true ice age of lock-in (Buizert and others, 2013). Past L is reconstructed directly from the SPC $\delta^{15}N$ data using the barometric equation (Sowers and others, 1992), where we apply a cubic spline for smoothness and assume a constant 4 m convective zone thickness. We use standard error propagation techniques to estimate the uncertainty in A from the uncertainties in the empirical Δage (Epifanio and others, 2020) and in L (set to 5 m). The resulting (1σ) uncertainty ranges from 5% to 15% of A. The A values reconstructed in this manner do not reflect the instantaneous values, but rather the values averaged over a time period corresponding the lifetime of the firn layer (ice equivalent, Δage). For the purpose of interpreting BNDs with respect to paleo-temperatures, this is actually the more meaningful parameter. Our accumulation record is shown in Fig. 5. Errors bars represent a root-mean-square (RMS) combination of the calculated gas-age/ice-age (Δage), and lock-in depth (L_{IE}) uncertainties.

https://doi.org/10.1017/aog.2025.10011 Published online by Cambridge University Press

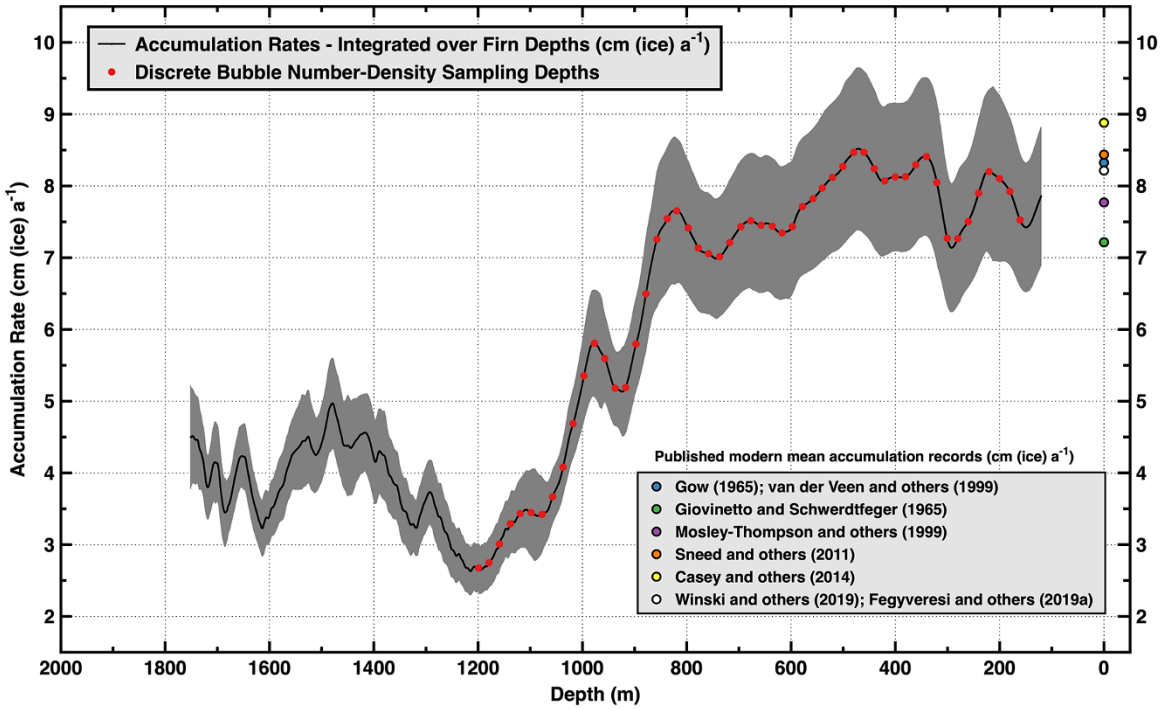


Figure 5. Firn-averaged accumulation (*A*) history (cm ice a^{-1}) for the South Pole site shown with combined uncertainty bands (gray) and discrete bubble number-density sampling depths (red). Published modern mean accumulation estimates are shown in ice-equivalent values.

4. Results and discussion

Paleotemperature reconstructions were calculated using the model developed by Spencer and others (2006) and incorporating the firn thickness accumulation record derived from the isotopic composition of N_2 ($\delta^{15}N\text{-}N_2$). We used the most recent dating of the SPC14 core that is based on volcanic electrochemical machining sulfate matching to the WAIS Divide core, together with annually resolved chemistry and visual stratigraphy (Winski and others, 2019), to convert sample depths to equivalent ages. This depth-age scale reveals that our samples do capture the entirety of the glacial–interglacial transition above the depth of clathrate-dominated ice (which affected our samples aged $>$ ~20 ka (ka bf 1950).

The published BND model of Spencer and others (2006) uses a bubble-per-grain ratio at close-off of $G = 2.02 \pm 0.08$, from a best fit to a suite of 15 data sets from sites with different temperatures and accumulation rates in Greenland and Antarctica. Some of the variability in their best-fit relation may arise from site-specific depositional effects, impurity effects, or influences of different ice-flow strain rates. None of these effects are large in the original study, and the technique yields useful results with the general multisite calibration; however, a site-specific calibration can largely remove any of these not-yet-quantified effects. The small difference between site-specific calibrations and the multisite calibration means that any time-evolution of the site-specific part of the calibration has a very small effect. Given the unique conditions for South Pole, including flank flow and uncertain history of ice-flow velocities, we conducted a detailed study of targeted samples across the South Pole pore close-off depth (~120 m) to determine a site-specific bubble-per-grain ratio, yielding a value of $G = 1.51 \pm 0.05$. While this value does not fall within the original study's published uncertainties, we feel this can be explained by the unique combination of site conditions for South Pole. This lower site-specific value of G serves primarily to shift the mean temperature of the reconstruction to more closely match estimated modern temperature at the site, with little effect on the calculated magnitude of temperature changes.

The resultant reconstruction using both the traditional bubble-section imagery and the micro-CT derived imagery reveals a warming across the late glacial–interglacial transition of ~7.5°C ± 0.87°C (Fig. 6). For each sample in the study, an integrated paleotemperature (representing the average temperature over the firnification time) was therefore determined using the measured BND, average accumulation rate for firnification time of the sample, and the steady-state model values of Spencer and others (2006). Combined error from the updated locally tuned model, the average accumulation rates, and estimated (RMS) mean bubble counting error of BND across our 53 traditional bubble-section samples (±17 bubbles cm^{-3}), gives an average temperature error of ±0.85°C. Combined error across our 11 micro-CT samples (±14 bubbles cm^{-3}) gives an average temperature error of ±0.89°C. These results support the use of 3-D micro-CT imagery in place of traditional bubble-section techniques as this approach more easily produced comparable temperature reconstructions with similar measures of uncertainty. Comparing the new empirical BND temperature estimate with water stable isotopes in the core implies an isotope-temperature regression slope of 0.97 ‰ $°C^{-1}$ for $\delta^{18}O_{ice}$ for the LGM-preindustrial difference.

We observed other noteworthy trends in our paleoclimate reconstruction. Our data reveal a relatively stable site temperature history through the Holocene at South Pole, with only a slight (<0.5°C) total warming—though with an upstream correction for deposition elevation the climatic temperature trend would be smaller or might disappear. This observation is consistent with several other published values for East Antarctic sites (e.g. Ciais and others, 1994; Stenni and others, 2004). Additionally, our data

https://doi.org/10.1017/aog.2025.10011 Published online by Cambridge University Press

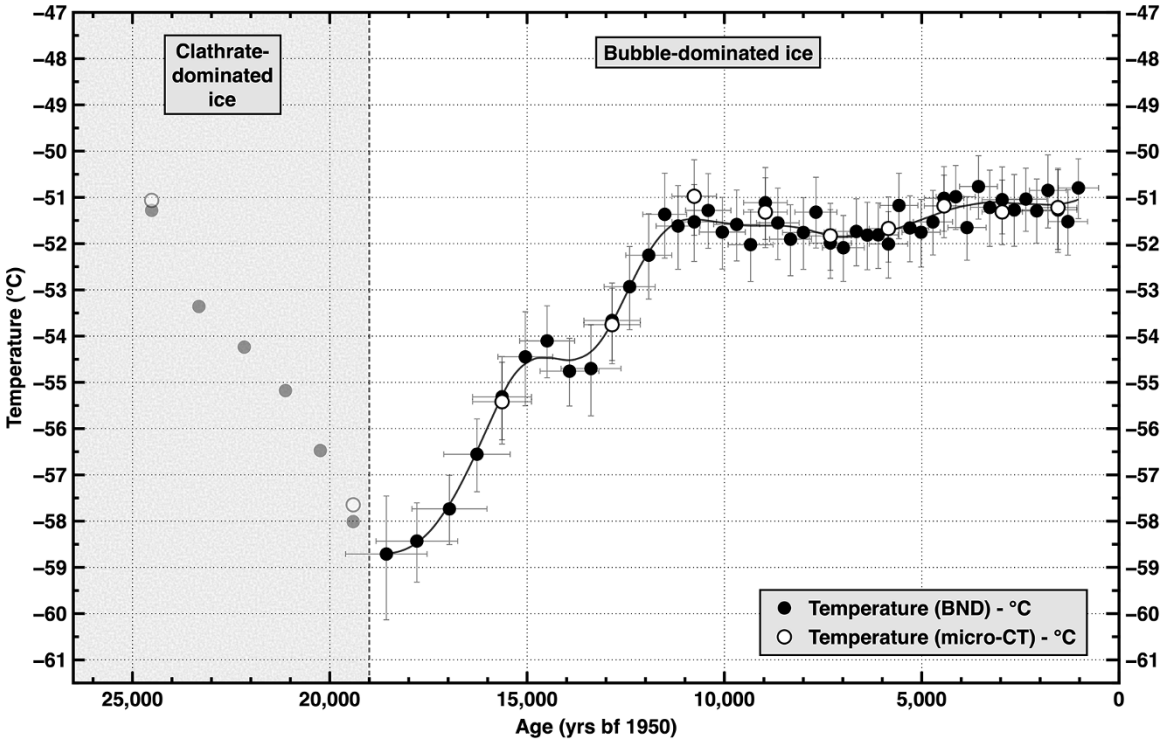


Figure 6. Past temperatures at the South Pole site, calculated from measured bubble number-density and accumulation rates. Horizontal 'error' bars represent the firnification time for each sample, and vertical error bars are the combined analytical errors, as described in the text. A LOESS smoothing line is shown to highlight major trends.

capture a clear Antarctic Cold Reversal (ACR) trend that closely matches the published timing estimates for a composite of six Antarctic sites by Pedro and others (2011), falling between their earliest ACR onset (14.80 ± 0.20 ka bf 1950) and latest ACR termination (13.02 ± 0.20 ka bf 1950). Lastly, and similar to our observations from WAIS Divide, the onset of clathrates became clear in samples below ~1100 m (aged > ~20 ka), and we therefore do not show those reconstructed paleotemperatures. Clathrates were observed in bubble-section samples in very small numbers as shallow as ~800 m, but were only abundant below ~1100 m, and therefore the presence of these clathrates did not significantly affect our analyses or reconstructions in shallower samples.

A decrease in accumulation rate often results from a decrease in temperature through dependence on the saturation vapor pressure, at ~7%°C^{-1} (Denton and others, 2005; Banta and others, 2008; Frieler and others, 2015). The linear regression observed in our South Pole data yields a relationship of ~13%°C^{-1} (R^2 = 0.88), however using log-scaled accumulation rates and the recently published methods by Nicola and others (2023), a regression yields 11%°C^{-1} (R^2 = 0.92; Fig. 7). This reveals a dependence greater than for thermodynamic control alone, suggesting contributions from dynamic processes, synoptic weather patterns, or changing ice sheet surface slopes. These values are consistent with the recent model-based studies that suggest a higher value (>10%°C^{-1}) in the Antarctic interior (Nicola and others, 2023).

Our modeled temperature history is consistent with other independent reconstructions for the site. As detailed above, our model estimates temperatures based on BND measurements from discrete depths in the core that are integrated over their respective pore close-off firn thicknesses, and corrected only for the effects of thinning. These estimates therefore represent temperatures during the time and at the place that the sample was in firn, such that older samples record conditions from farther upglacier. Temperature estimates reported by Buizert and others (2021a), and Kahle and others (2021) include data that are similarly uncorrected for upstream ice advection and therefore are used here for direct comparison.

Buizert and others (2021a) specifically distinguish three temperatures in their study: climatic temperature (T_{CLIM}), surface temperature (T_S) and vapor condensation temperature (T_C). In their study, they empirically reconstruct surface temperatures (T_S) by using either the isotopic composition of N_2 ($\delta^{15}N\text{-}N_2$) and empirically reconstructed Δage as noted above, or by inverting measured borehole temperatures. Upper and lower bounds of their reconstructed paleotemperatures reflect a Monte-Carlo estimation of the uncertainty in the method reflecting: (1) the firn densification model tuning and (2) the analytical uncertainty in the data used ($\delta^{15}N\text{-}N_2$ and empirical delta-age). As they reconstruct site temperature (T_S), their data are therefore comparable to our site temperatures estimated here. Data from Buizert and others (2021a), with published uncertainties, are shown for comparison to our data in Fig. 8a. In their study, they found a glacial–interglacial temperature difference at the South Pole site (reported as a cooling of the LGM as compared to the preindustrial period), to be 6.1°C ± 1.5°C consistent with an isotope scaling of 1.19 ‰ K^{-1}. Our estimate of ~7.5°C ± 0.87°C falls within the uncertainty bounds of their estimate.

Kahle and others (2021) use a novel approach to combine isotope diffusion length and other data sets from the SPC14 core to constrain temperature, accumulation-rate, and ice-thinning histories to estimated paleo-temperatures for South Pole. Their approach reveals a best-fit linear calibration between $\delta^{18}O$ and the mean of their reconstruction using a scaling of 0.99 ± 0.03 ‰°C^{-1} (2σ). Their published reconstruction using this best-fit calibration,

https://doi.org/10.1017/aog.2025.10011 Published online by Cambridge University Press

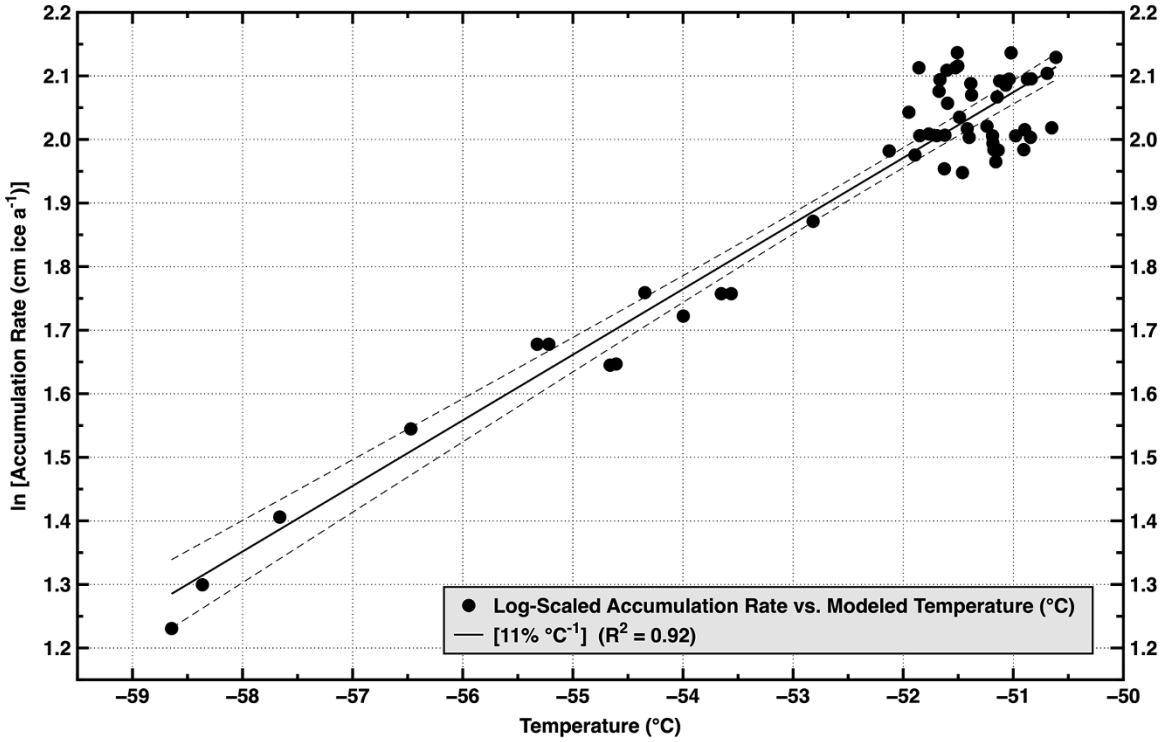


Figure 7. Estimates of log-scaled accumulation rates (cm ice a^{-1}) against the combined reconstructed temperatures (°C). Linear regression (with 95% confidence bands) yields a ~11% increase in accumulation rate per °C warming (R^2 = 0.92).

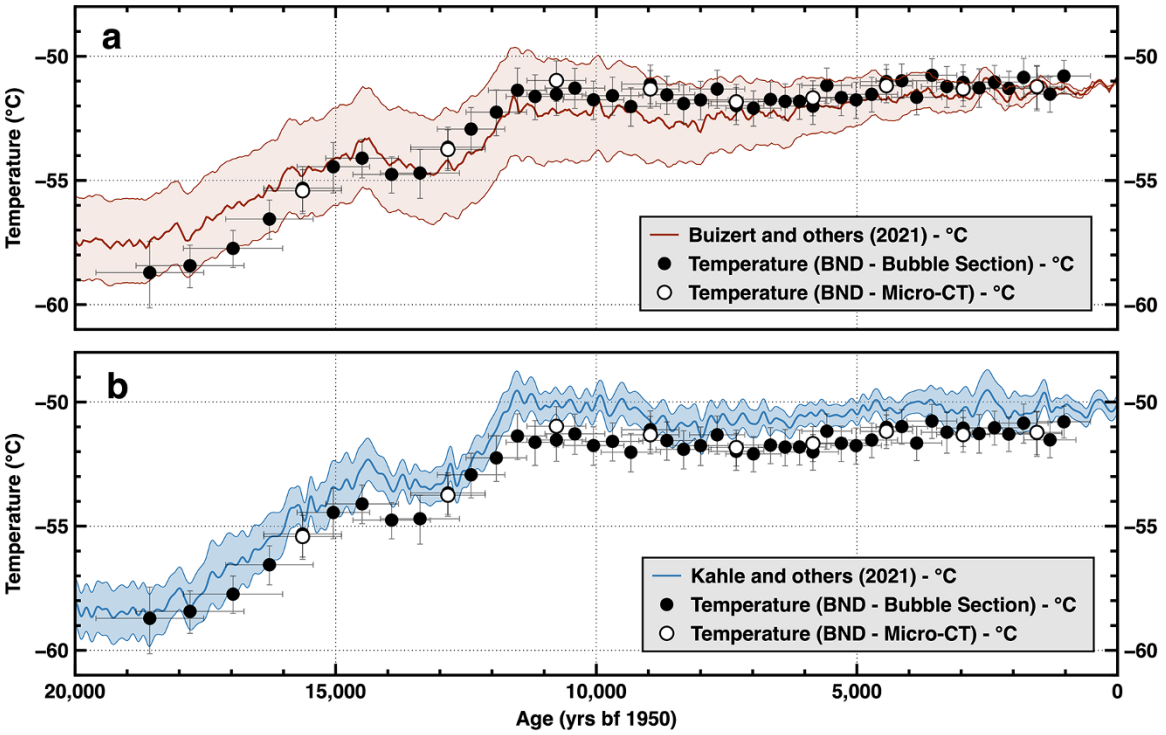


Figure 8. Modeled BND past temperatures at the South Pole site (from Figure 6) shown in panel (a) compared to surface temperatures (T_S) from Buizert and others (2021a)—derived from the isotopic composition of N_2 ($\delta^{15}N\text{-}N_2$), and in panel (b) compared to surface temperatures from Kahle and others (2021) – derived from $\delta^{18}o$ stable isotopes (0.99 ± 0.03 ‰°C^{-1} scaling), and destrained to correct for ice thinning.

and destrained to correct for ice thinning, is shown for comparison in Fig. 8b. In their work, Kahle and others (2021) note that while they used a diffusion length determined from the $\delta^{18}O$ power spectrum in the reconstruction, they did not use absolute $\delta^{18}O$ values.

https://doi.org/10.1017/aog.2025.10011 Published online by Cambridge University Press

As such, their results serve as a truly independent calibration of the traditional water-isotope thermometer, and as an excellent reconstruction for comparison here. Most notably, their site temperature reconstruction gives a glacial–interglacial temperature change at the South Pole site of 6.65 ± 0.96°C (1σ). Similar to the Buizert and others' (2021a) reconstruction noted above, our estimate of ~7.5°C ± 0.87°C also falls within the uncertainty bounds of this estimate.

The close agreement among the three histories is consistent with $\delta^{18}O$ providing a useful quantitative record of surface temperature and validates the use of BND as an independent measure of paleotemperatures. All three independent methods find temporal isotope sensitivities of ~ 1 ‰ °C^{-1} or greater, which is larger than the spatial regression slope of ~0.8 ‰ °C^{-1} (Masson-Delmotte and others 2008). We therefore conclude that the spatial regression slope method, as commonly used in Antarctic temperature reconstruction, overestimates the magnitude of glacial–interglacial temperature change at South Pole and possibly other locations.

Simple calculations using published ice velocities (~3–10 m a^{-1}) for South Pole (Lilien and others 2018) as well as estimates of surface slope (~0.0015) and dry adiabatic lapse rates (~10°C km^{-1}) indicate that almost all of the change in observed temperature across the transition is likely climatic, and not due to advection. Similar advection-corrected estimates were calculated by Kahle and others (2021) and found that upstream advection may account for at most, ~1°C of the measured difference temperature change across the transition.

Our results here also show that micro-CT measurements are comparable to those acquired through traditional methods, and therefore are appropriate for other ice-core derived estimates or reconstructions. Sample preparation and measurement via tomography is effectively nondestructive allowing for multiple and/or subsequent sample measurements. Traditional bubble-section preparation comes at the expense of significant ice loss through the microtoming process, and the resultant samples are limited to bubble-section analyses. Samples prepared for micro-CT measurement could be scanned multiple times and even repurposed for other co-registered physical, chemical, isotopic, or gas measurements. The micro-CT also allows bubble shape measurements, which may help in future studies following Fegyveresi and others (2019b) in use of bubbles as strain indicators.

Not only did the South Pole site allow the first successful implementation of the Spencer model across the glacial/interglacial transition, it also almost entirely avoids the difficulties posed by brittle ice. The South Pole Ice Core was remarkably stable upon recovery, exhibiting very minimal brittle-ice behavior. A subtle 'BIZ' was present within the SPC14 core within the depth interval of ~620–1080; however, the ice did not exhibit the typical brittle hallmarks upon recovery such as extreme cracking or spalling. (Souney and others 2021; Barnett and others, 2023). This notable lack of brittleness is most likely attributable to the unique site characteristics at South Pole, rather than the drilling and core handling procedures (Souney and others, 2021).

As noted above, Barnett and others (2023) and Fitzpatrick and others (2024) found that brittle-ice behavior is likely connected to fractures following chessboard subgrain boundaries within the ice, which are favored by large bubble and grain sizes. Consequently, at sites with small mean grain sizes and high BNDs such as South Pole, this may explain the observed lack of brittle-ice behavior. Given the minimal brittle behavior of the South Pole Ice core, it was an ideal candidate for the testing of the new micro-CT bubble measurements we present here, as the majority of our samples were intact and/or defect free.

5. Conclusions and future work

We applied the ice-core BND paleoclimate model developed by Spencer and others (2006) to new samples recovered from the South Pole Ice Core (SPC14), and found ~7.5°C ± 0.87°C warming from ~19.5 ka to the present from samples measured in the upper 1200 m of the core. This is the first successful application of this independent paleoclimate model across the most recent glacial/interglacial transition, made possible in large part by the minimal presence of brittle ice and the depth of significant clathrate onset (below ~1100 m). The data show a relatively stable Holocene (<0.5°C of warming) and a clear ACR signal (between ~15 and 13 ka). These findings agree closely with other published independent reconstructions for South Pole based on stable isotope measurements ($\delta^{15}N$ and $\delta^{18}O$), as well as published results from other East Antarctic sites (e.g. EPICA Dome C). Accumulation rate and modeled temperature varied together across our data sets (~11%°C^{-1}), suggesting contributions from dynamic processes, synoptic weather patterns, or changing ice sheet surface slopes.

We also show that using 3-D micro-CT imaging is a highly effective and comparable tool for measuring BND in core samples, and significantly reduces sample processing time when compared to traditional bubble-section techniques. This new method is also nondestructive to samples, preserving them for additional future analyses. Future analyses of bubble shape data, such as elongation orientation and aspect ratio, are planned in order to expand the work by Fegyveresi and others (2019b). We note that there currently does not exist any technique for capturing hybrid grain/bubble analyses in 3-D through micro-CT (or c-axis measurements); however, new methods are being continually developed that may further the potential for more expanded ice-core physical properties measurements.

Data availability statement. All data presented here are available through the request of the corresponding author, or via download from USAP-DC (10.15784/601880; Fegyveresi, 2025)

Acknowledgements. We acknowledge the following funding sources for support of this work: US National Science Foundation Division of Polar Programs grants 1542778, 1141839, 2315928 and 2218402. We also acknowledge Curt Labombard, Richard Nunn, and the staff of the National Science Foundation Ice Core Facility (NSF-ICF) in Denver, Colorado, as well as the South Pole Ice Core Coordination Office at the University of New Hampshire, and the Ice Drilling Design and Operations group at the University of Wisconsin. We thank numerous colleagues involved with the South Pole project, especially Eric Steig, Brad Markle, and Joe Souney. We thank all of the SPICEcore science technicians and core handlers for sample recovery. We also thank Samantha Barnett for assistance with the processing and interpretation of the bubble characterization data. Lastly, we thank our anonymous reviewers, whose thoughtful suggestions and questions served to clarify and improve this manuscript. Any use of trade, firm, or product names is for descriptive purposes only and does not imply endorsement.

Competing interests. The author(s) declare none.

References

Alley RB (2010) Reliability of ice-core science: Historical insights. *Journal of Glaciology* **56**(200), 1095–1103. doi:10.3189/002214311796406130

Alley RB and Fitzpatrick JJ (1999) Conditions for bubble elongation in cold ice-sheet ice. *Journal of Glaciology* **45**(149), 147–153. doi:10.1017/S0022143000003129

Bagherzadeh F, Freitag J, Frese U and Wilhelms F (2023) Ice-core micro-CT image segmentation with deep learning and Gaussian mixture model. *IEEE Transactions on Geoscience and Remote Sensing* **61**, 1–11. doi:10.1109/tgrs.2023.3334867

Bamber JL, Vaughan DG and Joughin I (2000) Widespread Complex Flow in the Interior of the Antarctic Ice Sheet. *Science* **287**(5456), 1248–1250. doi:10.1126/science.287.5456.1248

Banta JR, McConnell JR, Frey MM, Bales RC and Taylor K (2008) Spatial and temporal variability in snow accumulation at the West Antarctic Ice Sheet Divide over recent centuries. *Journal of Geophysical Research: Atmospheres* **113**(D23102), 1–8. doi:10.1029/2008JD010235

Barnett SM, Fegyveresi JM, Alley RB, Smith ME, Fitzpatrick JJ and Voigt DE (2023) Chessboard Subgrain Boundaries May Serve as Preferred Pathways for Ice-Fracture Propagation and Explain the Development of Brittle-Ice. *American Geophysical Union* **2023**(1447), C33E–1447.

Battle M and 10 others (1996) Atmospheric gas concentrations over the past century measured in air from firn at South Pole. *Nature* **383**(6597), 231–235. doi:10.1038/383231a0

Buizert C and 10 others (2015) The WAIS Divide deep ice core WD2014 chronology–Part 1: Methane synchronization (68–31 ka BP) and the gas age–ice age difference. *Climate of the Past* **11**(2), 153–173. doi:10.5194/cp-11-153-2015

Buizert C and 39 others (2021a) Antarctic surface temperature and elevation during the Last Glacial Maximum. *Science* **372**(6546), 1097–1101. doi:10.1126/science.abd2897

Buizert C (2021b) The ice core gas age-ice age difference as a proxy for surface temperature. *Geophysical Research Letters* **48**, e2021GL094241. doi:10.1029/2021gl094241

Buizert C, Sowers T and Blunier T (2013) Assessment of diffusive isotopic fractionation in polar firn, and application to ice core trace gas records. *Earth and Planetary Science Letters* **361**(2013), 110–119. doi:10.1016/j.epsl.2012.11.039

Casey KA, Fudge TJ, Neumann TA, Steig EJ, Cavitte MGP and Blankenship DD (2014) The 1500 m South Pole ice core: Recovering a 40 ka environmental record. *Annals of Glaciology* **55**(68), 137–146. doi:10.3189/2014aog68a016

Ciais P, Jouzel J, Petit JR, Lipenkov V and White JWC (1994) Holocene temperature variations inferred from Antarctic ice cores. *Annals of Glaciology* **20**, 427–436. doi:10.3189/172756494794587609

Cuffey KM and Paterson WSB (2010) *The Physics of Glaciers*, 4th edn. Oxford: Butterworth-Heinemann.

Dadic R and 7 others (2019) Temperature-driven bubble migration as a proxy for internal bubble pressures and bubble trapping function in ice cores. *Journal of Geophysical Research: Atmospheres* **124**(17-18), 10264–10282. doi:10.1029/2019JD030891

Denton GH, Alley RB, Comer GC and Broecker WS (2005) The role of seasonality in abrupt climate change. *Quaternary Science Reviews* **24**(10-11), 1159–1182. doi:10.1016/j.quascirev.2004.12.002

Epifanio JA and 16 others (2020) The SP19 chronology for the South Pole Ice Core–Part 2: Gas chronology, Δage, and smoothing of atmospheric records. *Climate of the Past* **16**(6), 2431–2444. doi:10.5194/cp-16-2431-2020

Epifanio JA and 8 others (2023) Millennial and orbital-scale variability in a 54 000-year record of total air content from the South Pole ice core. *Cryosphere* **17**(11), 4837–4851. doi:10.5194/tc-17-4837-2023

Fegyveresi JM and 7 others (2011) Late-Holocene climate evolution at the WAIS Divide site, West Antarctica: Bubble number-density estimates. *Journal of Glaciology* **57**(204), 629–638. doi:10.3189/002214311797409677

Fegyveresi JM and 7 others (2016) Five millennia of surface temperatures and ice core bubble characteristics from the WAIS Divide deep core, West Antarctica. *Paleoceanography* **31**(3), 416–433. doi:10.1002/2015PA002851

Fegyveresi JM (2025) South Pole Ice Core (SPC14) Bubble Number-Density Data. U.S. Antarctic Program (USAP). Data Center. Dataset. doi:10.15784/601880

Fegyveresi JM, Fudge TJ, Winski DA, Ferris DG and Alley RB (2019a) Visual Observations and Stratigraphy of the South Pole Ice Core (SPICEcore): A Chronology, *ERDC/CRREL Rep*. TR-19-10, 1–44, Hanover, NH, United States doi:10.21079/11681/33378

Fegyveresi JM, Alley RB, Voigt DE, Fitzpatrick JJ and Wilen LA (2019b) Instruments and methods: A case study of ice core bubbles as strain indicators. *Annals of Glaciology* **60**(78), 8–19. doi:10.1017/aog.2018.23

Fitzpatrick JJ, Wilen LA, Voigt DE, Alley RB and Fegyveresi JM (2024) Characteristics, origin, and significance of chessboard subgrain boundaries in the WAIS Divide Ice Core. *Annals of Glaciology* **66**(e12), 1–12. doi:10.1017/aog.2024.19

Frieler K and 8 others (2015) Consistent evidence of increasing Antarctic accumulation with warming. *Nature Climate Change* **5**(4), 348–352. doi:10.1038/nclimate2574

Fudge TJ and 8 others (2016) Variable relationship between accumulation and temperature in West Antarctica for the past 31,000 years. *Geophysical Research Letters* **48**(8), 3795–3803. doi:10.1002/2016GL068356

Fudge TJ and 8 others (2020) Advection and non-climate impacts on the South Pole Ice Core. *Climate of the Past* **16**(3), 819–832. doi:10.5194/cp-16-819-2020

Giovinetto MB and Schwerdtfeger W (1965) Analysis of a 200-year snow accumulation series from the South Pole. *Archives for Meteorology, Geophysics, and Bioclimatology, Series A* **15**(2), 227–250. doi:10.1007/BF02246754

Gow AJ (1965) On the Accumulation and Seasonal Stratification of Snow at the South Pole. *Journal of Glaciology* **5**(40), 467–477. doi:10.3189/S002214300001844X

Gow AJ (1968) Bubbles and bubble pressures in Antarctic glacier ice. *Journal of Glaciology* **7**(50), 167–182. doi:10.3189/S0022143000030975

Hagenmuller P, Chambon G, Lesaffre B, Flin F and Naaim M (2013) Energy-based binary segmentation of snow microtomographic images. *Journal of Glaciology* **59**(217), 859–873. doi:10.3189/2013JoG13J035

Hamilton GS (2004) Topographic control of regional accumulation rate variability at South Pole and implications for ice-core interpretation. *Annals of Glaciology* **39**, 214–218. doi:10.3189/172756404781814050

Kahle EC and 13 others (2021) Reconstruction of temperature, accumulation rate, and layer thinning from an ice core at South Pole, using a statistical inverse method. *Journal of Geophysical Research: Atmospheres* **126**(13), e2020JD033300. doi:10.1029/2020JD033300

Kuivinen K (1983) A 237-meter ice core from South Pole Station. *Antarctic Journal of the United States* **18**(5), 113–114.

Lilien DA and 7 others (2018) Holocene ice-flow speedup in the vicinity of the South Pole. *Geophysical Research Letters* **45**(13), 6557–6565. doi:10.1029/2018GL078253

Lipenkov VY (2000) Air bubbles and air-hydrate crystals in the Vostok ice core. In Hondoh T (ed), *Physics of Ice Core Records*. Sapporo: Hokkaido Univ. Press, 327–358.

Markle BR and Steig EJ (2022) Improving temperature reconstructions from ice-core water-isotope records. *Climate of the Past* **18**(6), 1321–1368. doi:10.5194/cp-18-1321-2022

Markle BR, Steig EJ, Roe GH, Winckler G and McConnell JR (2018) Concomitant variability in high-latitude aerosols, water isotopes and the hydrologic cycle. *Nature Geoscience* **11**(11), 853–859. doi:10.1038/s41561-018-0210-9

Martinerie P, Lipenkov VY and Raynaud D (1990) Correction of air-content measurements in polar ice for the effect of cut bubbles at the surface of the sample. *Journal of Glaciology* **36**(124), 299–303. doi:10.3189/002214390793701282

Masson-Delmotte V and 35 others (2008) A Review of Antarctic Surface Snow Isotopic Composition: Observations, Atmospheric Circulation, and Isotopic Modeling. *Journal of Climate* **21**(13), 3359–3387. doi:10.1175/2007JCLI2139.1

Morgan JD, Buizert C, Fudge TJ, Kawamura K, Severinghaus JP and Trudinger CM (2022) Gas isotope thermometry in the South Pole and Dome Fuji ice cores provides evidence for seasonal rectification of ice core gas records. *Cryosphere* **16**, 2947–2966. doi:10.5194/tc-16-2947-2022

Mosley-Thompson E, Paskievitch JF, Gow AJ and Thompson LG (1999) Late 20th Century increase in South Pole snow accumulation. *Journal of Geophysical Research: Atmospheres* **104**(D4), 3877–3886. doi:10.1029/1998jd200092

Nicola L, Notz D and Winkelmann R (2023) Revisiting temperature sensitivity: How does Antarctic precipitation change with temperature? *Cryosphere* **17**(7), 2563–2583. doi:10.5194/tc-17-2563-2023

Nye J (1963) Correction factor for accumulation measured by the thickness of the annual layers in an ice sheet. *Journal of Glaciology* **4**(36), 785–788. doi:10.3189/S0022143000028367

Palais JM, Kyle PR, Mosley-Thompson E and Thomas E (1987) Correlation of a 3,200-year-old tephra in ice cores from Vostok and South Pole Stations, Antarctica. *Geophysical Research Letters* **14**(8), 804–807. doi:10.1029/GL014i008p00804

Parrenin F and 8 others (2012) On the gas-ice depth difference (Δdepth) along the EPICA Dome C ice core. *Climate of the Past* **8**, 1239–1255. doi:10.5194/cp-8-1239-2012)

Pedro JB and 7 others (2011) The last deglaciation: Timing the bipolar seesaw. *Climate of the Past* **7**(2), 671–683. doi:10.5194/cp-7-671-2011

Saltykov SA (1976) *Stereographic Metallography*. Moscow: Metallurgia.

Schneider DP and Steig EJ (2008) Ice cores record significant 1940s Antarctic warmth related to tropical climate variability. *Proceedings of the National Academy of Sciences of the United States of America* **105**(34), 12154–12158. doi:10.1073/pnas.0803627105

Sigl M and 26 others (2016) The WAIS Divide deep ice core WD2014 chronology–Part 2: Annual-layer counting (0–31 ka BP). *Climate of the Past* **12**, 769–786. doi:10.5194/cp-12-769-2016)

Sneed SB, Mayewski PA and Dixon DA (2011) An emerging technique: Multi-ice-core multi-parameter correlations with Antarctic sea-ice extent. *Annals of Glaciology* **52**(57), 347–354. doi:10.3189/172756411795931822

Souney JM and 13 others (2021) Core handling, transportation and processing for the South Pole ice core (SPICEcore) project. *Annals of Glaciology* **62**(84), 118–130. doi:10.1017/aog.2020.80

Sowers T, Bender M, Raynaud D and Korotkevich YS (1992) $\delta^{15}N$ of N_2 in air trapped in polar ice: A tracer of gas transport in the firn and a possible constraint on ice age-gas age differences. *Journal of Geophysical Research* **97**(D14), 15683–15697. doi:10.1029/92JD01297

Spencer MK, Alley RB and Creyts TT (2001) Preliminary firn-densification model with 38-site dataset. *Journal of Glaciology* **47**(159), 671–676. doi:10.3189/172756501781831765

Spencer MK, Alley RB and Fitzpatrick JJ (2006) Developing a bubble number-density paleoclimatic indicator for glacier ice. *Journal of Glaciology* **52**(178), 358–364. doi:10.3189/172756506781828638

Steig EJ and 8 others (2021) Continuous-Flow Analysis of $\delta^{17}O$, $\delta^{18}O$, and δD of H_2O on an Ice Core from the South Pole. *Frontiers of Earth Science* **9**, 640292. doi:10.3389/feart.2021.640292)

Steig EJ, Schneider DP, Rutherford SD, Mann ME, Comiso JC and Shindell DT (2009) Warming of the Antarctic ice-sheet surface since the 1957 International Geophysical Year. *Nature* **457**(7228), 459–462. doi:10.1038/nature07669

Stenni B and 13 others (2004) A late-glacial high-resolution site and source temperature record derived from the EPICA Dome C isotope records (East Antarctica). *Earth and Planetary Science Letters* **217**(1-2), 183–195. doi:10.1016/S0012-821X(03)00574-0

Ueltzhöffer KJ and 6 others (2010) Distribution of air bubbles in the EDML and EDC (Antarctica) ice cores, using a new method of automatic image analysis. *Journal of Glaciology* **56**(196), 339–348. doi:10.3189/002214310791968511

Vandecrux B and 65 others (2023) The SUMup collaborative database: Surface mass balance, subsurface temperature and density measurements from the Greenland and Antarctic ice sheets (1912–2023), NSF Arctic Data Center. doi:10.18739/A2M61BR5M

Van der Veen CJ, Mosley-Thompson E, Gow AJ and Mark BG (1999) Accumulation at South Pole: Comparison of Two 900-Year Records. *Journal of Geophysical Research: Atmospheres* **104**(D24), 31067–31076. doi:10.1029/1999JD900501

Winski DA and 30 others (2019) The SP19 chronology for the South Pole Ice Core–Part 1: Volcanic matching and annual layer counting. *Climate of the Past* **15**(5), 1793–1808. doi:10.5194/cp-15-1793-2019

Winski DA and 13 others (2021) Seasonally resolved Holocene sea-ice variability inferred from South Pole ice core chemistry. *Geophysical Research Letters* **48**(8), e2020GL091602. doi:10.1029/2020GL091602

https://doi.org/10.1017/aog.2025.10011 Published online by Cambridge University Press